Maximum Stable Bubble Size and Gas Holdup in High-Pressure Slurry Bubble Columns

Xukun Luo, D. J. Lee, Raymond Lau, Guoqiang Yang, and Liang-Shih Fan
Dept. of Chemical Engineering, The Ohio State University, Columbus, OH 43210

Experiments of pressure effects on gas holdup and bubble size in slurry bubble columns at 5.6 MPa and at gas velocities up to 45 cm/s indicate that the gas holdup increases with an increase in pressure, especially at high slurry concentration. At ambient pressure, a higher solids concentration significantly lowers gas holdup over the entire gas-velocity range, while at 5.6 MPa, the effect of solids concentration on gas holdup is relatively small at gas velocities above 25 cm/s. An empirical correlation was developed based on these data and those in the literature to predict gas holdup in bubble and slurry bubble columns over a wide range of operating conditions. An analysis of bubble flow characteristics during dynamic gas disengagement indicates that large bubbles play a key role in determining gas holdup due to the large bubble and wake volumes that induce the acceleration of small bubbles. Direct measurement of bubble size shows that elevated pressures lead to smaller bubble size and narrower bubble-size distributions. Bubble size increases significantly with increasing solids concentration at ambient pressure, while at high pressures this effect is less pronounced. A theoretical analysis of circulation of gas inside the bubble yields an analytical expression for maximum stable bubble size in high-pressure slurry bubble columns. Based on this internal circulation model, the maximum stable bubble size at high pressures is significantly smaller due to the high gas inertia and low gas−liquid surface tension. The smaller bubble size and its reduced bubble rise velocity account for the observed pressure effect on gas holdup.

Introduction

The applications of slurry bubble column reactors in methanol and Fischer−Tropsch syntheses have gained considerable attention in recent years (Fox, 1990; Saxena, 1995; Krishna et al., 1997). These reactors are typically operated at elevated pressures (1.0−8.0 MPa) and at high superficial gas velocities (~ 30 cm/s). The design and scale-up of these reactors require comprehensive knowledge of the hydrodynamics under these operating conditions. The fundamentals of the hydrodynamics have been extensively studied over the past decades and comprehensive literature reviews are available (Shah et al., 1982; Fan, 1989; Deckwer, 1992; Saxena and Chen, 1994). However, most studies were conducted under ambient pressure conditions, and relatively little is known regarding the hydrodynamics at high pressures with relevance to industrial processes.

Gas holdup is a key parameter that characterizes the transport phenomena of bubble column systems. The gas holdup generally increases with an increase in gas velocity, with a larger increasing rate in the dispersed bubble regime than in the churn-turbulent regime. The distributor design affects the gas holdup significantly only at low gas velocities. In bubble columns, the effect of column size on gas holdup is negligible when the column diameter is larger than 0.1−0.15 m (Shah et al., 1982). The influence of the column height is insignificant if the height is above 1−3 meters and the ratio of the column height to the diameter is larger than 5 (Kastaneck et al., 1984). The gas holdup decreases as liquid viscosity and/or gas−liquid surface tension increase. The addition of particles into a bubble column leads to a larger bubble size and thus a decreased gas holdup, especially when the particle concentration is low. The particle size effect on the gas holdup can be neglected in the particle-size range of 44−254 μm.

Correspondence concerning this article should be addressed to L.-S. Fan.

Some studies have been conducted to investigate the effect of pressure on the gas holdup of bubble columns (Tarmy et al., 1984; Idogawa, 1986; Wilkinson et al., 1992; Deckwer and Schumpe, 1993; Reilly et al., 1994; Jiang et al., 1995; Lin et al., 1998) and three-phase fluidized beds (Luo et al., 1997a). It is commonly accepted that elevated pressures lead to higher gas holdups in both bubble columns and three-phase fluidized beds except in those systems that are operated with porous plate distributors and at low gas velocities. The increased gas holdup is directly related to the smaller bubble size and, to a lesser extent, the slower bubble rise velocity at higher pressures (Luo et al., 1997b). The most fundamental reason for the bubble size reduction can be attributed to the variation in physical properties of the gas and liquid with pressure. Three mechanisms are involved: smaller initial bubble size from the gas distributor (larger gas density), reduced bubble coalescence rate (lower surface tension and larger liquid viscosity), and increased bubble breakup rate (larger gas density and smaller surface tension). Empirical correlations have been proposed for the gas holdup in bubble columns operated at elevated pressure and temperature (Wilkinson et al., 1992; Reilly et al., 1994).

Significant pressure effects on the gas holdup should exist in slurry bubble columns; however, little is reported concerning such effects. Deckwer et al. (1980) found little effect of pressure on the gas holdup in a Fischer–Tropsch slurry bubble column with a porous plate distributor ($P = 0.4–1.1$ MPa; $T = 143–260$°C; $U_g = 0–3.5$ cm/s). The experimental data of Kojima et al. (1991) indicated that the gas holdup increases with the pressure; but no pressure effect was observed at the 30 wt. % solids concentration ($P = 0.1–1.1$ MPa, $U_g = 1.7–9$ cm/s, single-orifice distributor). Inga (1997) measured the gas holdup in slurry bubble columns for Fischer–Tropsch synthesis at pressures up to 0.72 MPa, and a significant pressure effect was observed. No viable model or correlation is currently available to predict the gas holdup in high-pressure slurry bubble columns.

The knowledge of bubble flow characteristics and bubble size is essential to a fundamental understanding of gas holdup behavior in slurry bubble columns. Lee et al. (1998) studied the flow structure and the bubble characteristics in bubble columns utilizing the particle image velocimetry (PIV) and dynamic gas disengagement (DGD) techniques. The DGD technique was first used in bubble columns at low gas velocities ($U_g < 2$ cm/s) by Sriram and Mann (1977) to quantify the bubble size and size distribution in the columns. Various models that relate gas disengagement phenomena to bubble size or size distribution have been proposed in the literature (Vermeer and Krishna, 1981; Schumpe and Grund, 1986; Patel et al., 1989; Daly et al., 1992). However, the reliability of the DGD technique applied to the slurry bubble columns operated at high pressure and high gas velocity depends on whether the models account for the transient characteristics of bubble flow during the DGD process. Little has been reported on the evolutions of the instantaneous distributions of the bubble size and bubble rise velocity during the gas disengagement process.

The objective of this work is to investigate the effects of pressure on the hydrodynamics of slurry bubble columns under conditions of industrial relevance. In this study, experiments are conducted to measure gas holdup at pressures up to 5.6 MPa and at gas velocities up to 45 cm/s. An empirical correlation is developed to account for the gas holdup behavior in high-pressure slurry bubble columns. The PIV system is applied to examine the flow characteristics and to substantiate the applicability of the DGD technique for the measurement of the bubble-size distribution in the slurry bubble column operated under the present conditions. The bubble size and its distribution are directly measured using a fiber-optic probe in the high-pressure slurry bubble column. A mechanistic model is proposed to illustrate the bubble breakup mechanism at high pressures. The mechanism is verified by comparing the model predictions of maximum stable bubble size with the experimental data.

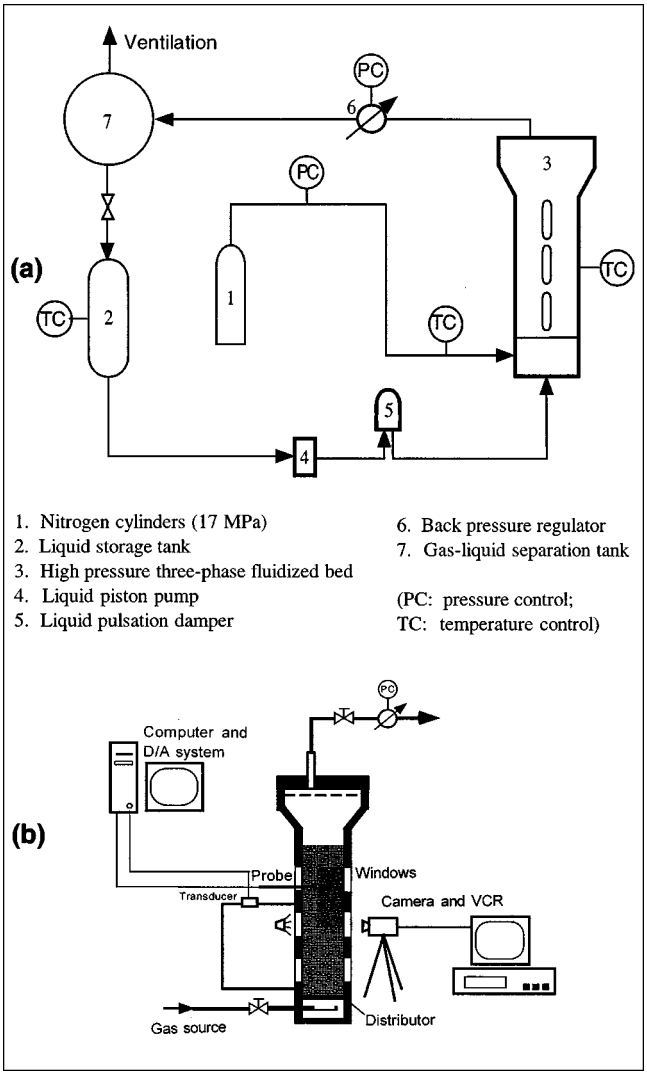

Figure 1. (a) High-pressure multiphase flow and visualization system; (b) high-pressure slurry bubble column and instrumentation setup.

Experimental Studies

High-pressure slurry bubble column and gas holdup measurement

The experiments are conducted in a high-pressure multiphase flow and visualization system, as shown in Figure 1.

Table 1. Physical Properties of the Paratherm NF Heat-Transfer Fluid

P (MPa)	ρ_g (kg/m^3)	ρ_l (kg/m^3)	μ_l (Pa·s)	σ_l (N/m)
		(a) $T = 28$°C		
0.1	1.13	870	0.026	0.029
1.48	16.5	872	0.028	0.028
2.86	32.0	874	0.031	0.027
5.62	62.8	878	0.034	0.026
		(b) $T = 78$°C		
0.1	0.97	846	0.0051	0.026
1.48	14.2	850	0.0054	0.024
2.86	27.4	852	0.0056	0.023
5.62	53.9	857	0.0059	0.021

The maximum operating pressure and temperature of this system are 21 MPa and 180°C, respectively. The high-pressure slurry bubble column is 0.102 m in diameter and 1.37 m in height. The column is divided into three sections: plenum region, test section, and disengagement section. Three pairs of quartz windows are installed on the front and rear sides of the column. Each window is 12.7 mm in width and 93 mm in height. The windows cover the entire test section. A perforated plate is used as the gas distributor, with 120 square-pitched holes of 1.5-mm diameter. The volume of the plenum region beneath the distributor is 1.18 L.

In this study, the liquid is in batch mode. Nitrogen from the high-pressure cylinders is introduced into the slurry bubble column after the pressure and temperature are adjusted to desired values. The gas exiting from the column flows through a back-pressure regulator and is vented into an exhaust system. The back-pressure regulator controls the system pressure. The gas flow rate is measured using a high-pressure turbine flowmeter. In this study, Paratherm NF heat transfer fluid is used as the liquid phase. The physical properties of this liquid are shown in Table 1. The solids phase is alumina particles with a wet density of 2,440 kg/m^3. The particle sizes are uniformly distributed between 90 μm and 110 μm with an averaged diameter of 100 μm. The clear liquid level is maintained at 0.5 m above the distributor. Experiments are performed in two slurries of different solids volume fractions (ϕ_s) of 0.081 and 0.191.

The gas holdup in the slurry bubble column is measured using the dynamic gas disengagement technique. After the flow in the column reaches steady state, the gas inlet and outlet are simultaneously shut off to maintain constant system pressure. The bubbles disengage from the column and the particles gradually settle down. A differential pressure transducer is used to monitor the variation of the dynamic pressure drop during the process. The positive port of the transducer is located at 0.18 m above the distributor, while the negative port is located at 0.36 m above the distributor.

Figure 2 shows an example of the differential pressure signal during the disengagement process. The column is at steady state before the gas flow is shut off at $t = 9.0$ s. It can be seen from the figure that the entire process can be divided into six stages: (1) immediately following gas shutoff, a sudden jump of the differential pressure signal corresponds to the simultaneous disengagement of bubbles of all sizes; (2) the increase of the signal value is much more gradual, since only relatively small bubbles escape from the column; (3) the differential pressure remains at a relatively constant value for a period of about 150 s because the particles are still fully suspended by the liquid motion induced by bubbles; (4) starting from $t = 150$ s, the pressure drop increases gradually. During this time period, the liquid motion dies down and particles start settling down, which leads to an increased solids concentration in the region between the two pressure ports. A solids surface can be seen to move downward at this stage; (5) the solids surface continues to move down and drops into the region between the two pressure ports, which causes a steep drop in the differential pressure value ($550 < t < 800$ s); (6) the particle surface is below the lower pressure port ($t > 800$ s) and the pressure drop approaches zero.

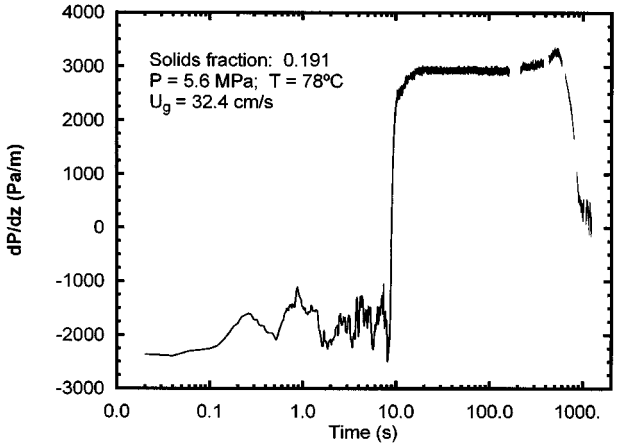

Figure 2. Variation of dynamic pressure drop with time in a bed-collapse process.

The gas holdup can then be calculated from the dynamic pressure drops at the steady state together with that at stage (3). The ratio of the solids holdup to the liquid holdup, K, remains constant in the region between the two pressure ports from the initial stage to stage (3). The dynamic pressure drop in stage (3) can be approximated as

$$\left(\frac{\Delta P}{\Delta z}\right)_d^0 = (\rho_l \epsilon_l^0 + \rho_s \epsilon_s^0 - \rho_l) g = \epsilon_s^0 (\rho_s - \rho_l) g. \quad (1)$$

Fu et al. (1995) used a similar equation to measure the solids holdup in slurry bubble columns. Based on Eq. 1, K can be written as

$$K = \frac{\epsilon_s}{\epsilon_l} = \frac{(\Delta P/\Delta z)_d^0}{(\rho_s - \rho_l) g - (\Delta P/\Delta z)_d^0}. \quad (2)$$

With K known, the differential pressure signals at steady state and at bubble escape can be related to the phase holdups and densities of the three phases by

$$\left(\frac{\Delta P}{\Delta z}\right)_d = (\rho_g \epsilon_g + \rho_l \epsilon_l + \rho_s \epsilon_s - \rho_l) g = \left\{ \frac{K(\rho_s - \rho_l)}{1+K} + \left[\frac{(1+K)\rho_g - (\rho_l + K\rho_s)}{1+K} \right] \epsilon_g \right\} g. \quad (3)$$

Solving Eq. 3 for ϵ_g and replacing K with Eq. 2 yields

$$\epsilon_g = \frac{\left[(\Delta P/\Delta z)_d^0 - (\Delta P/\Delta z)_d\right]/g}{(\Delta P/\Delta z)_d^0/g + (\rho_l - \rho_g)}. \quad (4)$$

The particle density is not present in Eq. 4; hence, the gas holdup can be calculated without knowledge of the particle density. The advantage of this technique is that the gas holdup and solids holdup can be evaluated simultaneously when the particle density is known. The solids concentration in the slurry bubble column can also be monitored with this method to ensure that all the particles are completely suspended at various gas velocities.

Bubble flow characteristics and bubble-size measurement

PIV Measurements in DGB Process. Dynamic gas disengagement experiments are conducted in a two-dimensional (2-D) Plexiglas column under ambient conditions as well as in a 3-D column under high pressures. The instantaneous flow fields during the DGD process are analyzed using a PIV system to study the characteristics of bubble flow and to examine the assumptions used in the existing DGD models. The detailed experimental setup for the 2-D column is given in Lee et al. (1998). In the 2-D column, the liquid phase used is tap water, and is operated under batch conditions with the static liquid height maintained at 120 cm. Compressed air and alumina particles of 100 μm mean diameter are used as the gas and solid phases, respectively. After steady-state operation is reached, the gas supply is shut off with a three-way valve, with one outlet being connected to the atmosphere, to prevent trickling bubbles from leaking into the column after shutoff.

The image of the flow field during the DGD process is recorded with a high framing-rate and high-resolution CCD camera equipped with a variable electronic shutter ranging from 1/60 to 1/10,000 s. A framing rate of 240 fields/s is used in this study. The PIV system used here was originally developed by Chen and Fan (1992), and was enhanced and modified to measure instantaneous full-field flow characteristics for a given plane. The modified PIV technique has sufficient accuracy to determine time/volume averaged flow information for each phase including velocities and dispersed phase-size distributions. Further, the PIV technique developed for multiphase systems has the ability to discriminate between the different phases, and provides the instantaneous, full-field flow properties of each phase. With the PIV system, the transient flow behavior during the DGD process can be analyzed and compared to the assumptions made in various models.

Fiber-Optic Probe Measurement. Direct measurements of bubble sizes in the high-pressure slurry bubble column are conducted using a fiber-optic probe. The probe utilizes the difference in refractive index of gas and liquid to distinguish the gas phase from the liquid–solid suspension. The probe is U-shaped, similar to that of de Lasa et al. (1982). There are variations in the tip designs for U-shaped probes used by various researchers to obtain maximum internal light reflection intensity for multiphase flow measurements. In the present probe, the fiber cladding in the tip portion is partially removed in such a manner that it yields the most distinctive signals for gas void detection. The cross section of the tip perpendicular to the flow direction in this probe has a dimension of 1.2×4 mm. The output of the photomultiplier is interfaced with a computer data-acquisition system, which samples the signal for four seconds at a frequency of 2,000 Hz. The tip of the probe is located at the center of the column and 0.35 m above the distributor.

The probe is calibrated in a chain of bubbles, that is, the bubbles passing through the tip periodically. The bubble rise velocity, u_b, can be calculated by

$$u_b = \frac{\Delta h}{\Delta \tau_2}, \quad (5)$$

where Δh is the vertical distance between the two tips, and $\Delta \tau_2$ is the time lag between the rear surface of the bubbles intercepting the upper and lower tips. The result is calibrated against the bubble rise velocity measured with a video camera. It is noted that $\Delta \tau_2$ is consistently less than the other time lag, $\Delta \tau_1$, corresponding to the frontal surface, due to the deformation of the frontal surface upon the interception. The comparison between the two bubble velocities reveals that $\Delta \tau_2$ should be used instead of $\Delta \tau_1$. The average error for the bubble rise velocity by the probe is less than 5%. The bubble chord length, l, is evaluated as

$$l = u_b \tau \quad (6)$$

where τ is the time period when the bubble is in contact with the lower tip of the probe. The probe actually measures the vertical chord length of the bubble rather than the bubble diameter.

Results and Discussion

Overall gas holdup

Figures 3 through 6 show the gas holdup in the slurry bubble columns under various temperature, solids concentration, and pressure conditions. Two temperatures of 28°C and 78°C are considered in the experiments. Specifically, the effect of the solids concentration on the gas holdup is shown in Figure 3. The presence of particles reduces the gas holdup at both the ambient and 5.6 MPa pressures, especially when the solids fraction is increased from 0 to 0.081. At ambient pressure, the gas holdup in the bubble column ($\phi_s = 0$) is almost 100% higher than in the slurry of 0.191 solids volume fraction over the entire gas velocity range. In contrast, at the pressure of 5.6 MPa, the effect of the solids concentration on the gas holdup is relatively small at gas velocities above 25 cm/s. For example, at 5.6 MPa, the gas holdup decreases from 0.55 to 0.48 (12%) as the solids fraction increases from 0 to 0.191 at a constant gas velocity of 30 cm/s; while at ambient pressure the gas holdup decreases from 0.35 to 0.18 (49%) for the same solids concentration increase and at the same gas velocity.

The pressure effect on the gas holdup can be seen in Figures 4–6. In general, elevated pressures lead to higher gas holdups under all the experimental conditions in the present study. The pressure effect is more significant at low pressures. Examination of the pressure effect on gas holdup at

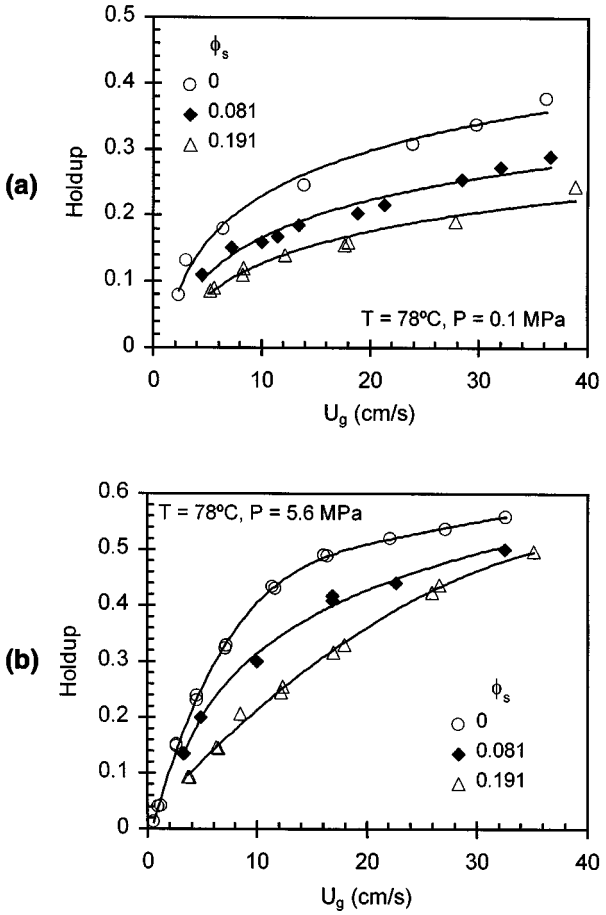

Figure 3. Effect of solids concentration on the gas holdup at two pressures: (a) $P = 0.1$ MPa; (b) $P = 5.6$ MPa.

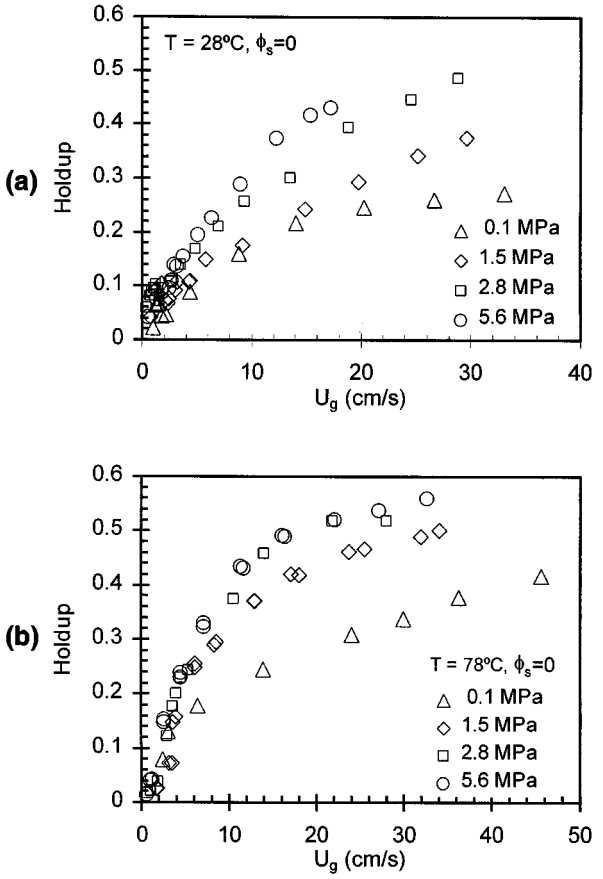

Figure 4. Gas holdup as a function of gas velocity at various pressures and temperatures in a bubble column ($\phi_s = 0$): (a) $T = 28$°C; (b) $T = 78$°C.

different solids concentrations indicates that the pressure effect is more pronounced at higher solids concentrations. For example, at a gas velocity of 30 cm/s and a temperature of 78°C, the gas holdup increases from 0.34 to 0.55 (62% increase) in the bubble column ($\phi_s = 0$) when the pressure is elevated from 0.1 MPa to 5.6 MPa. At the same gas velocity and temperature, and for the same pressure change, the gas holdup changes from 0.25 to 0.49 (96%) in the slurry system with a solids fraction of 0.081, and from 0.2 to 0.45 (125%) in the slurry system with a solids concentration of 0.191.

For design purposes, an empirical correlation is developed to account for the gas holdup in high-pressure slurry bubble columns operated in the coalesced bubble regime, as given below:

$$\frac{\epsilon_g}{1-\epsilon_g} = \frac{2.9\left(\frac{U_g^4 \rho_g}{\sigma g}\right)^{\alpha}\left(\frac{\rho_g}{\rho_{sl}}\right)^{\beta}}{\left[\cosh\left(Mo_{sl}^{0.054}\right)\right]^{4.1}}, \qquad (7)$$

where Mo_{sl} is the modified Morton number for the slurry phase, $(\xi\mu_l)^4 g/\rho_{sl}\sigma^3$, and

$$\alpha = 0.21\, Mo_{sl}^{0.0079} \quad \text{and} \quad \beta = 0.096\, Mo_{sl}^{-0.011}, \qquad (7a)$$

where ρ_g and σ are, respectively, the gas density and gas–liquid surface tension at operating pressure and temperature. The effective slurry density, ρ_{sl}, is given by

$$\rho_{sl} = \phi_s \rho_s + \phi_l \rho_l \qquad (8)$$

where ϕ_s and ϕ_l are the volume fractions of the solids and the liquid in the gas-free slurry. In Eq. 7, ξ is a correction factor which accounts for the effect of particles on slurry viscosity:

$$\ln \xi = 4.6\phi_s\left\{5.7\phi_s^{0.58} \sinh\left[-0.71 \exp(-5.8\phi_s) \ln Mo^{0.22}\right] + 1\right\}, \qquad (9)$$

where Mo is the Morton number of the liquid, $g\mu_l^4/\rho_l\sigma^3$. When the solids volume fraction approaches zero, this correlation reduces to the form for bubble columns. The correlation takes into account not only the experimental data obtained in this work, but also the data obtained in systems of various gas, liquid, and solids used by different authors. Table 2 lists the various experimental systems and their correspond-

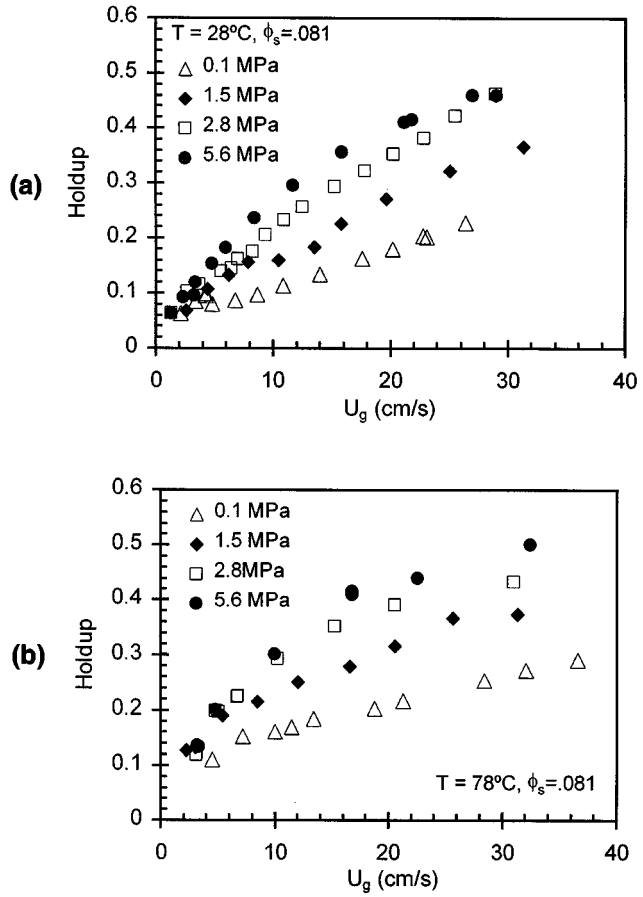

Figure 5. Gas holdup as a function of gas velocity at various pressures and temperatures in a slurry bubble column (ϕ_s = 0.081): (a) T = 28°C; (b) T = 78°C.

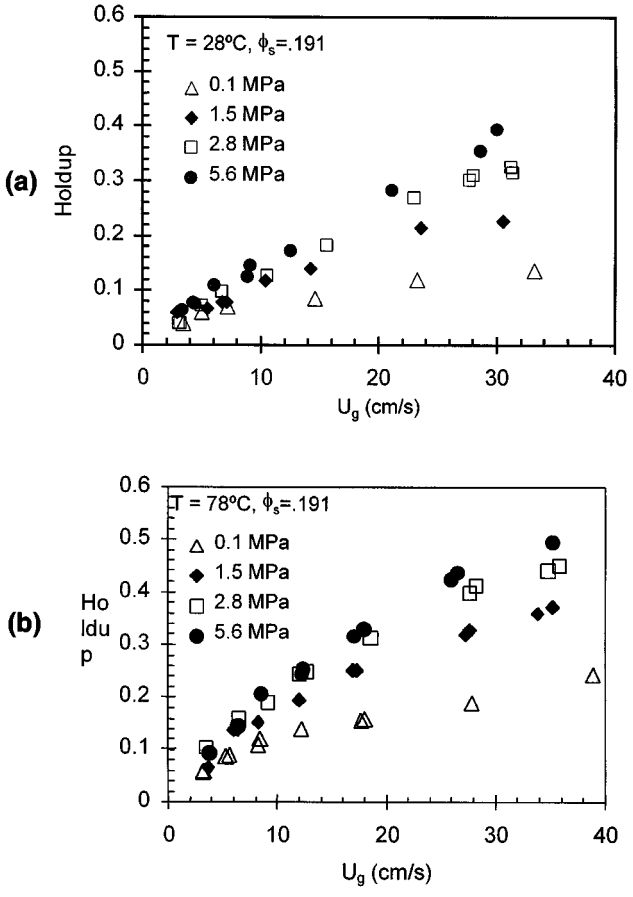

Figure 6. Gas holdup as a function of gas velocity at various pressures and temperatures in a bubble column (ϕ_s = 0.191): (a) T = 28°C; (b) T = 78°C.

ing references. The column diameter in the selected systems is larger than 0.1 m and the ratio of column height to diameter is larger than 5. The gas distributors are perforated plate, sparger, or bubble cap distributor. The average error of the predictions is 13% for both the slurry and gas–liquid systems and the maximum error is 53%. Figure 7 shows the comparison between the predictions by the correlation and experimental data. Oyevaar (1989) measured the gas holdup of an air/water system at pressures up to 7.8 MPa in a column of 0.08-m diameter. Although the error of the predictions by the correlation is 40% at ambient pressure, the error at the high pressure is only 10%, which implies that the scale effect on the gas holdup is relatively small at high pressures due to the smaller bubble sizes. The applicable ranges of the correlation are summarized in Table 3.

Flow characteristics and bubble-size distribution

Flow Characteristics from DGD Experiments. To fundamentally explain the effect of pressure on the gas holdup in the slurry bubble column, it is essential to understand the flow characteristics and the bubble-size variation with the pressure in the system. The frame-by-frame analysis of the instantaneous flow fields of the bubble phase reveals the importance of the interaction between the small and large bubbles. A wake is formed when the bubble Reynolds number is above 20 for a single bubble (Fan and Tsuchiya, 1990). The wake behind the bubble generates a low-pressure region. Smaller bubbles are frequently attracted into the region and are accelerated to almost the same rise velocity as the leading bubble. This attraction phenomenon is evident in the results obtained from the DGD experiments. Figures 8a and 8b show the variations of the number of the largest bubbles and the number of bubbles with the largest rise velocity during a DGD process. As the number of the large bubbles gradually decreases during the DGD process, so does the rise velocity of the small bubbles. It is noted that the bubbles larger than 2.0 cm rise at velocities of approximately 50 cm/s. The initial number of bubbles with rise velocity larger than 50 cm/s is around 12, while the initial number of bubbles larger than 2.0 cm is only 2. Further, the number of fast rising bubbles becomes zero only after the largest bubbles completely disengage at 1.5 s. The preceding observations clearly show the bubble-wake attraction effect. Without such attraction only the largest bubbles can reach this high velocity. Note that the superficial gas velocity in Figure 8 is 3.0 cm/s; as the superfi-

Table 2. Various Experimental Systems and References Selected

Gas/Liquid/Solids Systems	References	Symbols in Figure 7
Air/methanol, air/water, air/glycol, He/water, CO_2/water	Akita and Yoshida (1973)	—
Air/tetrabromoethane, air/*n*-octanol, air/ethylene glcyol, air/butan-diol(1,3)	Bach and Pilhofer (1978)	–
CH_4/C6/FeOx, CO/C6/FeOx, N_2/C6/FeO$_x$, H_2/C6/FeOx	Inga (1997)	□
Air/water, air/water/glass beads	Kiode et al. (1984)	+
Air/water, N_2/water, N_2/turpentine, N_2/butanol, N_2/MEG	Krishna et al. (1991)	▲
Air/water/glass beads	Li and Prakash (1997)	◇
N_2/water/glass beads	O'Dowd et al. (1987) Saxena et al. (1989)	□
Nitrogen/water	Oyevaar (1989)	■
N_2/water	Petukhov and Kolokol'tsev (1965)	△
Air/Isopar G, He/water, air/water, air/trichloroethylene	Reilly et al. (1994)	×
N_2/Drakeol-10/ZnO_x, N_2/Drakeol-10/CuO_x, N_2/Drakeol-10/Alumina	Schollenberger and O'Hern (1997)	△
N_2/*n*-heptane	Tarmy et al. (1984)	◆
N_2/*n*-heptane, N_2/MEG, N_2/water	Wilkinson et al. (1992)	○

cial gas velocity increases, the effect of the large bubbles on the rise velocity of the smaller bubbles becomes more dominant. Lee et al. (1998) studied the amount of the small bubbles attracted by the large bubbles with the PIV system in a 2-D bubble column at various superficial gas velocities. They concluded that at gas velocities above 11 cm/s, over 70% of the initial small bubbles disengage from the column with the large bubbles; at gas velocities below 4 cm/s, the number is around 20%. The preceding observations undoubtedly indicate the dominant effect of the large bubbles on the rise velocity of the bubbles in bubble columns and slurry bubble columns. Moreover, the volume of a bubble is proportional to the cube of the bubble size. Since the gas holdup is basically dictated by the size and rise velocity of bubbles, the large bubbles play a key role in determining the gas holdup in these systems.

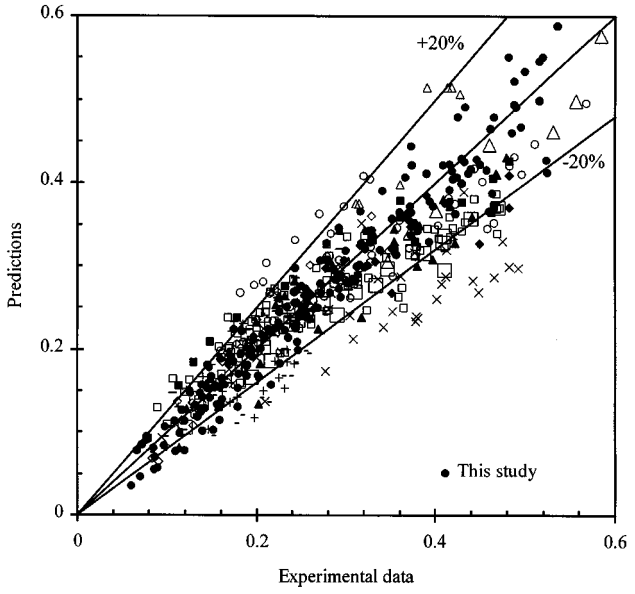

Figure 7. Comparison between the predicted gas holdup and the experimental data.

The significance of the bubble-wake attraction calls for examination of the existing models that describe the DGD profiles, that is, the gas holdup or liquid height variation with time during the DGD process. The various existing DGD models are summarized in Figure 9, in which the gas is shut off at t_0. If a bimodal bubble-size distribution is assumed, the DGD profile can be approximated by two straight lines. The line with a steeper slope corresponds to the escape of both large and small bubbles in stage (1) as discussed earlier; the other line corresponds to the escape of the small bubbles in stage (2). If the rise velocity of the small bubbles is assumed to be constant throughout the entire disengagement process, the line for stage 2 can be extrapolated to t_0 to obtain the initial holdup of the small bubbles (Sriram and Mann, 1977), marked as Model 1 in Figure 9. If it is assumed that the small bubbles do not disengage in stage (1) due to the liquid backflow (Model 2), the initial small-bubble holdup is simply the gas holdup at t_1, that is, at the end of stage 1 (Vermeer and Krishna, 1981). The other assumption made regarding the disengagement rate of bubbles is that the slip velocity be-

Table 3. Applicable Range of the Gas Holdup Correlation

Parameter (Units)	Range
ρ_l (kg/m^3)	668–2965
μ_l (mPa·s)	0.29–30
σ_l (N/m)	0.019–0.073
ρ_g (kg/m^3)	0.2–90
ϕ_s	0–0.4
d_p (μm)	20–143
ρ_s (kg/m^3)	2200–5730
U_g (m/s)	0.05–0.69
U_l (m/s)	0 (batch liquid)
D_c (m)	0.1–0.61
H/D_c	> 5
Distributor types	Perforated plate, sparger, and bubble cap

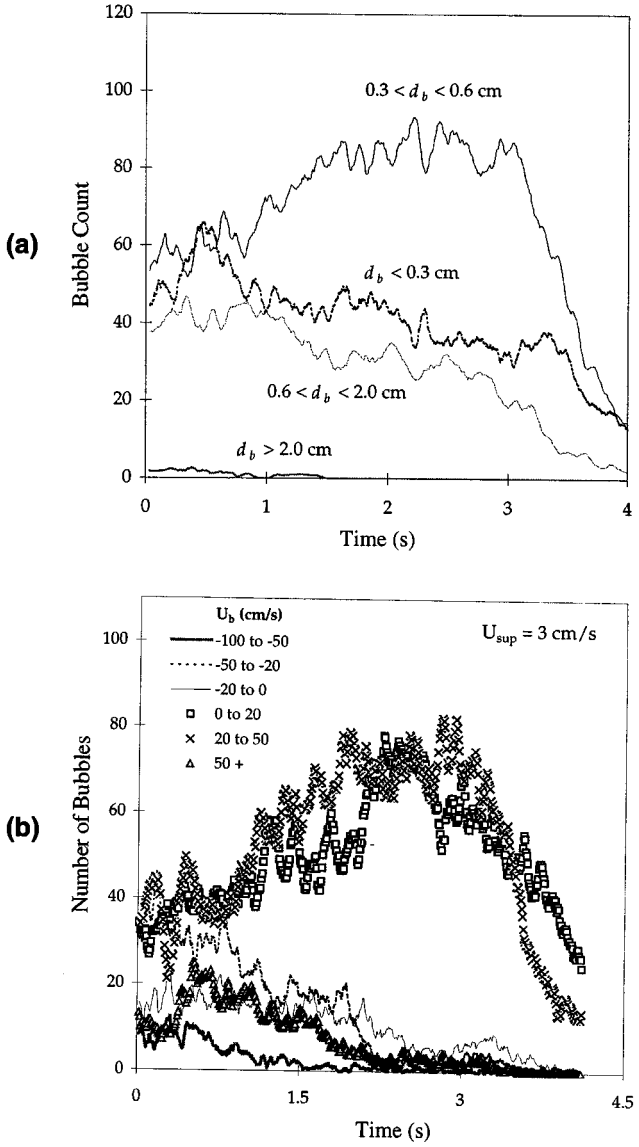

Figure 8. Bubble flow characteristics during a DGD process: (a) bubble-size variation (U_g = 3.0 cm/s, from Lee et al., 1998); (b) bubble rise velocity variation.

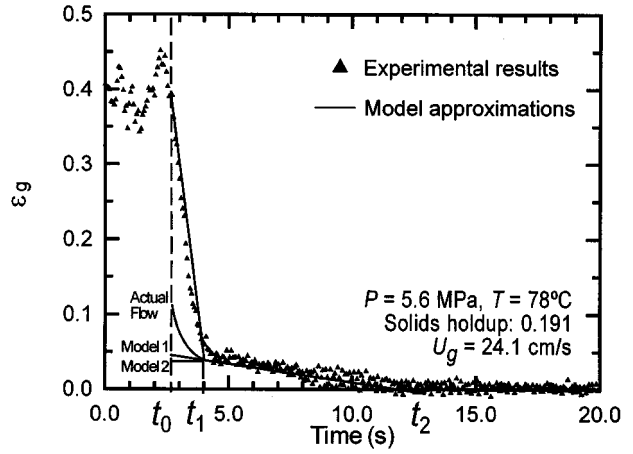

Figure 9. Characteristics of models 1 and 2 in accounting for the experimental gas holdup variation during the gas disengagement process.

tween the gas and the liquid is constant (Patel et al., 1989). In this case, the calculated small-bubble holdup falls in between the values of Model 1 and Model 2. However, since all the three assumptions regarding the small-bubble rise velocity do not recognize the bubble acceleration due to the large bubbles at the first stage, the models may lead to errors in estimating holdups for both small and large bubbles, especially at high superficial gas velocities, as shown in Figure 9. The preceding analysis is based on a bimodal bubble-size assumption; the true bubble disengagement behavior is even more complex as the bubble-size distribution is known to be continuous. The liquid circulation in the column further complicates the analysis of the DGD processes (Desphande et al., 1995).

In addition to the bubble-wake attraction, strong bubble coalescence and breakup are also observed during the DGD process, which invalidates the first assumption made in the existing DGD models, that is, no bubble coalescence and breakup. However, the error due to this assumption is minimal if a dynamic equilibrium between the bubble coalescence and the bubble breakup can be assumed.

In summary, the intrinsic bubble flow behavior in the dynamic gas disengagement process is complex in nature. Through the bubble wake attraction, the gas holdups in bubble columns or slurry bubble columns are closely associated with the size and number of the large bubbles. A fundamental explanation of the pressure effect on gas holdup should be based on a full understanding of the variation of bubble size, especially of the large-bubble size, with the pressure. The existing DGD models can only provide preliminary estimations about the holdup structure and bubble-size distribution in slurry bubble columns at low gas velocities. In slurry bubble column reactors operated at high gas velocities, such as those in the methanol synthesis process, the bubble-size distribution cannot be reasonably estimated by the DGD technique without the quantification of bubble–bubble interactions. Therefore, direct measurement is the only accurate means to quantify bubble-size distribution.

Pressure Effect on Bubble Size. A fiber-optic probe can give a reliable measurement of the bubble-size distribution in the high-pressure slurry bubble column. It is noted that the probe can only measure the bubble chord length instead of the true bubble diameter. If a uniform bubble shape is assumed (either spherical or ellipsoidal), the bubble chord length distribution can be converted to the size distribution (Liu et al., 1996). However, the bubbles in slurry bubble columns have irregular shapes. The data from the probe can thus only represent the chord-length distribution.

Special attention should be placed on the maximum chord length for the dominant effect of large bubbles on the gas holdup. In addition, the measured maximum chord length can be interpreted as the height of the largest bubble (h_{max}) in the system if the number of bubbles detected by the probe is

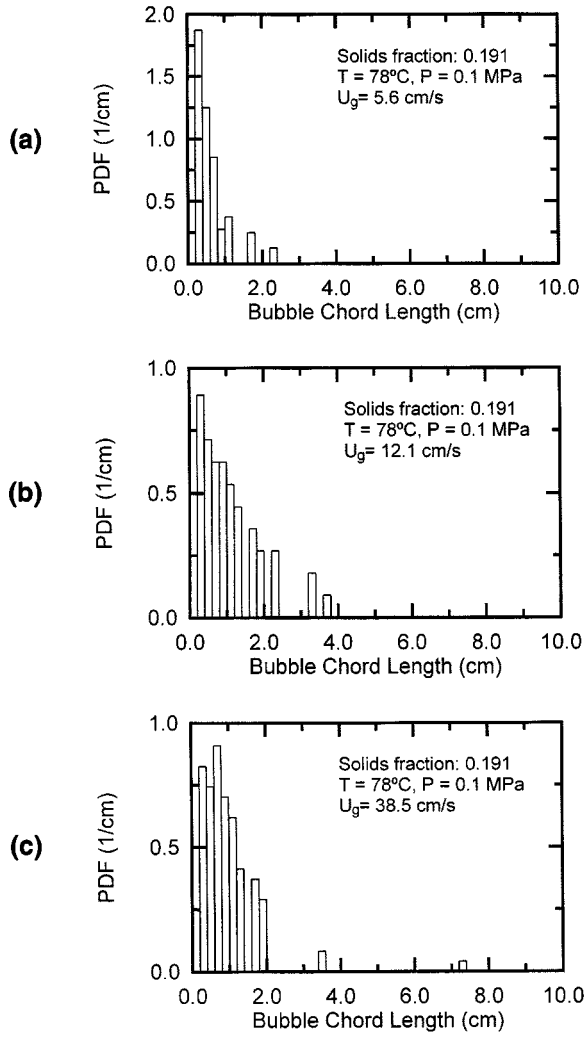

Figure 10. Bubble-size distribution in the slurry bubble column at ambient pressure.

large enough. In general, the maximum bubble height differs from the maximum bubble size. Nevertheless, the large bubbles in 2-D slurry bubble columns of different solids concentrations have approximately the same maximum dimensions in the horizontal and vertical directions, based on the photos shown by de Swart et al. (1996) and observations from the 2-D experiments. The maximum bubble size can thus be approximated by the maximum bubble height in 2-D slurry bubble columns. It is further assumed here that this approximation also holds for 3-D columns; thus, the maximum bubble chord length is approximated as the maximum bubble diameter in the following analysis.

Figure 10 shows the bubble chord-length distributions of a slurry at ambient pressure. The *y*-axis and the *x*-axis represent the probability density distribution function and the bubble-chord length in the vertical direction, respectively. It can be seen that the bubbles at ambient pressure have a wide size distribution. The maximum bubble size increases with an increase in gas velocity. The maximum bubble size is about 7.2 cm at a gas velocity of 38.5 cm/s. The slurry bubble column is apparently operated in the slugging regime. The slugging regime is also confirmed by a visual observation of the flow through the quartz windows. The periodical penetration of light is evident from the opposite-side lighting in the experiments. At high gas holdup, for the ambient-pressure case, the column is opaque except for a flash of light as the large bubble rises past the window. In contrast, for the 5.6 MPa case, the column is opaque over the entire gas velocity range. This indicates a much smaller bubble size in the high-pressure case. A comparison of the data shown in Figures 10 and 11 indicates that pressure has a significant effect on the breakage of the large bubbles. At a pressure of 5.6 MPa, the bubble size is much smaller and the bubble-size distribution is narrower, similar to the results obtained in high-pressure bubble columns and three-phase fluidized beds. The maximum bubble size is around 2.4 cm at a gas velocity of 37.4 cm/s. In addition to the bubble-size reduction, bubbles rise at slower velocities at high pressures. The increase in gas holdup with pressure is a consequence of the decreases both in the bubble size and in the bubble rise velocity, that is, larger bubbles broken into smaller ones and their rise velocities further reduced by pressure.

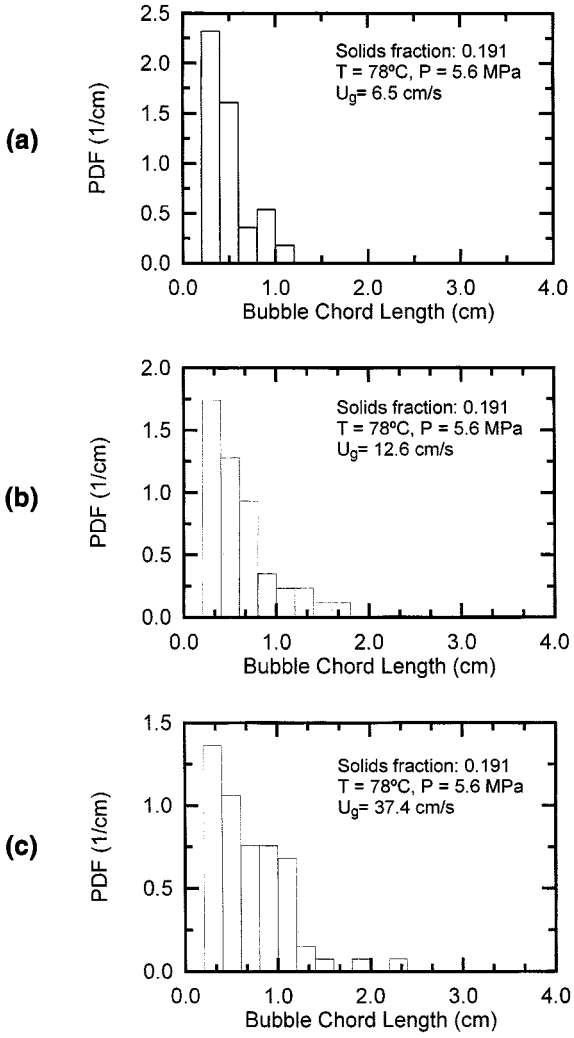

Figure 11. Bubble-size distribution in the slurry bubble column at a pressure of 5.6 MPa.

The maximum bubble size under different conditions can be seen from Figure 12. Under otherwise constant conditions, the maximum bubble size decreases with an increase in pressure, especially at pressures lower than 1.5 MPa. Increasing particle concentration leads to significantly larger bubble sizes at ambient pressure over the entire gas velocity range. On the other hand, the particle concentration has a significant effect on the maximum bubble size only in the gas velocity range of 8–23 cm/s at the pressure of 5.6 MPa. At gas velocities above that range, the maximum bubble size is virtually independent of solids concentration. Due to the dominant role of the large bubbles in determining the gas holdup, the preceding observation can explain the similar solids concentrations effect on gas holdup shown in Figure 3. The effect of solids concentration on gas holdup is significant over the entire gas velocity range at ambient pressure; the solids concentration effect on gas holdup is relatively small at gas velocities above 25 cm/s at the pressure of 5.6 MPa.

Maximum Stable Bubble Size: Background. The upper limit of the bubble size is set by the maximum stable bubble size, D_{max}, above which the bubble is subjected to breakup and is hence unstable. Several mechanisms have been proposed to predict the maximum stable bubble size in gas–liquid systems. Hinze (1955) proposed that the bubble breakup is caused by the dynamic pressure and the shear stresses on the bubble surface induced by different liquid flow patterns, for example, shear flow and turbulence. When the maximum hydrodynamic force in the liquid is larger than the surface tension force, the bubble disintegrates into smaller bubbles. This mechanism can be quantified by the liquid Weber number; when the Weber number $= \rho_l \overline{u^2} D_{max}/\sigma$ is larger than a critical value, the bubble is not stable and disintegrates. This theory was adopted to predict the breakup of bubbles in gas–liquid systems (Walter and Blanch, 1986). Calculations by Lin et al. (1998) showed that the theory underpredicts the maximum bubble size and cannot predict the observed effect of pressure on bubble size.

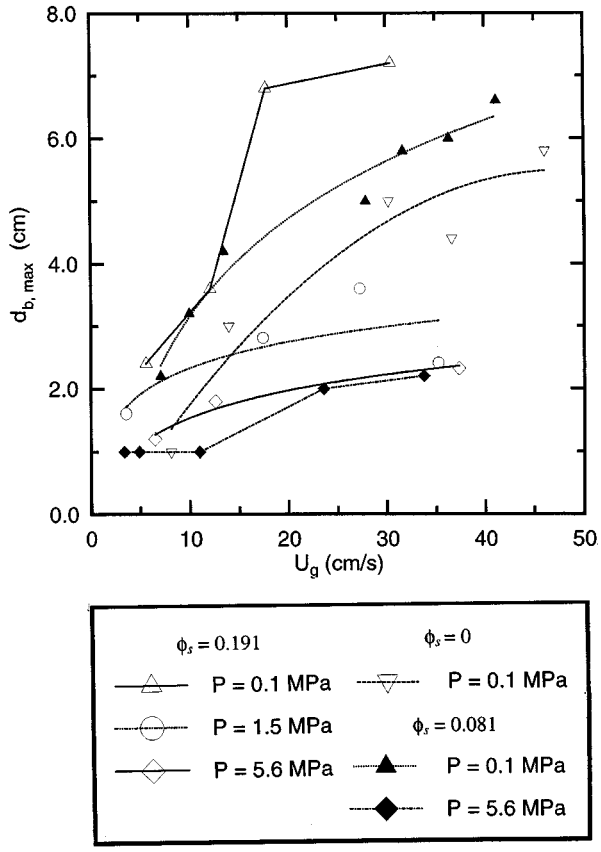

Figure 12. Effect of pressure on maximum bubble size in a slurry bubble column (T = 78°C).

A maximum stable bubble size exists for bubbles rising freely in a stagnant liquid without the external stresses (Grace et al., 1978). The Rayleigh–Taylor instability has been regarded as the mechanism for the bubble breakup under such conditions. A horizontal interface between two stationary fluids is unstable with respect to disturbances having wavelengths exceeding a critical value if the upper fluid has a higher density than the lower one (Bellman and Pennington, 1954). Chen and Fan (1988) obtained an expression for the critical wavelength for a curved surface as in the case of bubble. Grace et al. (1978) applied the Rayleigh–Taylor instability theory by considering the time available for the disturbance to grow and the time required for the disturbance to grow to an adequate amplitude. Batchelor (1987) pointed out that the observed maximum air bubbles in water were considerably larger than that predicted by the model of Grace et al. (1978). Batchelor (1987) further took into account the stabilizing effects of the liquid acceleration along the bubble surface and the nonconstant growth rate of the disturbance. In his model, the information of disturbances is required for the prediction of the maximum bubble size. The models based on the Rayleigh–Taylor instability predict an almost negligible pressure effect on the maximum bubble size; in fact, the Rayleigh–Taylor instability implies that the bubble is slightly more stable when the gas density is higher.

Kitscha and Kocamustafaogullari (1989) applied the Kelvin–Helmholtz instability theory to model the breakup of large bubbles in liquids, using the same concept of Grace et al. (1978). Wilkinson and Van Dierendonck (1990) applied the critical wavelength to explain the maximum stable bubble size in high-pressure bubble columns. Their results showed that the critical wavelength decreases with an increase in pressure, and therefore bubbles are easier to disintegrate by the disturbances. However, the critical wavelength is not necessarily equivalent to the maximum stable bubble size and their approach alone cannot quantify the pressure effect on bubble size.

All the models mentioned earlier neglected the effect of the internal circulation of the gas. For the continuity of the tangential velocity in the gas and liquid phases, the internal circulation velocity is of the same order of magnitude as the bubble rise velocity. A centrifugal force is induced by this circulation, pointing outwards to the bubble surface, which can suppress the disturbances at the gas–liquid interface and act as a stabilizing force. This force may be another reason to explain the underestimation of D_{max} by the model of Grace et al. (1978), besides that discussed by Batchelor (1987). On the other hand, centrifugal force can also disintegrate the bubble as it increases with an increase in bubble size. The bubble breaks up when the centrifugal forces exceeds the

surface-tension force, especially at high pressures when gas density is high.

Levich (1962) recognized the fact of internal gas circulation and assumed the centrifugal force to be equal to the dynamic pressure induced by the gas moving at the bubble rise velocity, and proposed a simple equation to calculate the maximum stable bubble size:

$$D_{\max} \approx \frac{3.63\sigma}{u_b^2 \sqrt[3]{\rho_l^2 \rho_g}}. \tag{10}$$

Equation 10 shows a significant effect of pressure on the maximum bubble size; however, it severely underpredicts the maximum bubble size.

Maximum Stable Bubble Size: Proposed Mechanistic Model. An analytical criterion for the bubble breakup can be derived by considering a single large bubble rising in a stagnant liquid at a velocity of u_b, without any disturbances on the gas–liquid interface. The bubble is subjected to breakup when its size exceeds the maximum stable bubble size due to the circulation and centrifugal force. Large bubbles normally assume a spherical cap shape; in this work, the spherical cap bubble is approximated by an ellipsoidal bubble with the same volume and the same aspect ratio (height to width). The bubble is described in a cylindrical coordinate system that moves with the bubble and has the center of the ellipsoidal bubble as its origin, as shown in Figure 13a. The bubble surface is formed by rotating an ellipse around the vertical axis, z:

$$\frac{r_c^2}{a^2} + \frac{z^2}{c^2} = 1, \tag{11}$$

where r_c is the distance from the z-axis. The aspect ratio of the ellipse ($\alpha = c/a$) is the same as that of the real spherical cap bubble. The internal circulation can be described by Hill's vortex (Hill, 1894), because of the high Reynolds number of the gas in the bubble. The flow field is symmetrical about the z-axis and has no azimuthal component. The circulation velocity in the r_c and z-directions are, respectively,

$$u = \frac{3u_b}{2c^2} z r_c = \frac{3u_b}{2\alpha^2 a^2} z r_c \tag{12a}$$

and

$$w = \frac{3u_b}{2a^2}\left[\left(a^2 - 2r_c^2\right) - \frac{z^2}{\alpha^2}\right]. \tag{12b}$$

In the presence of contaminants, a small bubble would behave like a rigid particle, and thus the circulation of the gas inside the bubble could be suppressed. For large bubbles, as encountered in the model, the high shear force generated by the high relative velocity between the bubble and the liquid or slurry could readily sweep away the contaminants on the surface, and thus the contaminants induce negligible effects on the internal circulation of the gas (Levich, 1962).

To model the bubble breakup, it is necessary to evaluate the x-component of the centrifugal force, F_x, on the entire bubble surface, as shown in Figure 13c. Based on Eqs. 12a and 12b, there is a surface within the bubble S, on which the z-component of the circulation velocity, w, is zero and the circulation velocity has only the component in the r_c direction, u, as shown in Figures 13a and 13b. This surface can be described as

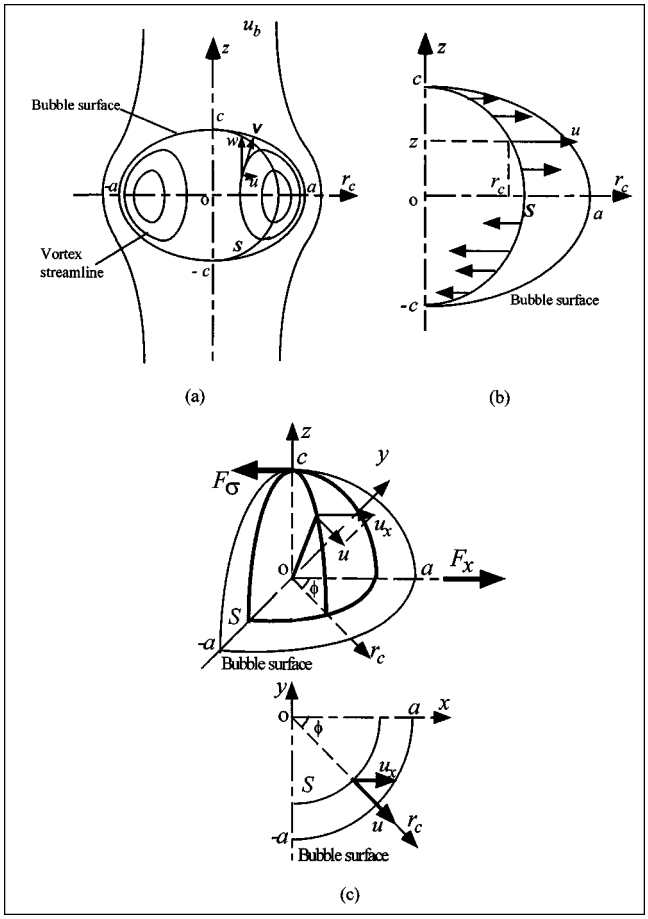

Figure 13. Internal circulation model for bubble breakup: (a) internal and external flow fields; (b) circulation velocity on surface *S*; (c) force balance and 3-D view of surface *S* and the flow pattern on *S*.

$$\frac{2r_c^2}{a^2} + \frac{z^2}{\alpha^2 a^2} = 1. \tag{13}$$

Surface S passes through the vortex center and intercepts all the vortex streamlines, as shown in Figure 13a. Because the pressure field inside the bubble is symmetrical about the x-y plane, F_x is simply the rate of change of momentum across the surface S in the x-direction, based on a momentum balance for the gas phase. In addition, the streamlines inside the bubble are symmetrical about the x-y plane and x-z plane, and thus, F_x is four times the rate of the x-component of the gas momentum flowing across an octant of surface S shown in Figure 13c,

$$F_x = 4\iint_S \left(\rho_g u \cdot \delta S\right) u_x = 4\rho_g \iint_S u^2 \cos\phi \, r_c \, d\phi \, dz, \tag{14}$$

where ($\rho_g u \cdot \delta S$) is the mass flow rate across a surface element of S. Substituting Eq. 12a into Eq. 14 and integrating the resulting equation yields F_x:

$$F_x = 4\rho_g \int_0^{\pi/2} \cos\phi \, d\phi \int_0^c \left(\frac{3u_b z r_c}{2\alpha^2 a^2} \right)^2 r_c \, dz$$

$$= 4\rho_g \int_0^c \left(\frac{3u_b z r_c}{2c^2} \right)^2 r_c \, dz = \frac{9\rho_g u_b^2}{\alpha^4 a^4} \int_0^c r_c^3 z^2 \, dz. \quad (14a)$$

From Eq. 13, r_c can be expressed as

$$r_c = \sqrt{\frac{1}{2}\left[a^2 - \left(\frac{z}{\alpha} \right)^2 \right]}. \quad (15)$$

Substituting Eq. 15 into Eq. 14a and integrating the resulting equation yields F_x:

$$F_x = \frac{9\rho_g u_b^2}{2\sqrt{2}\,\alpha^4 a^4} \int_0^c z^2 \left[a^2 - \left(\frac{z}{\alpha} \right)^2 \right]^{3/2} dz$$

$$= \frac{9\pi}{64\sqrt{2}\,\alpha} \rho_g u_b^2 a^2 = \frac{0.312}{\alpha} \rho_g u_b^2 a^2. \quad (16)$$

The surface tension force is the product of the surface tension and the circumference of the ellipse described by Eq. 11,

$$F_\sigma = \sigma L = \sigma \int_{\text{ellipse}} \sqrt{(\delta r_c)^2 + (\delta z)^2} = 4\sigma a E\left(\sqrt{1-\alpha^2}\right), \quad (17)$$

where $E(\sqrt{1-\alpha^2})$ is the complete second kind elliptic integral, which decreases with a decrease in α. Also, the volume equivalent bubble diameter, d_e, is related to a and α by

$$\frac{\pi}{6} d_e^3 = \frac{4\pi}{3} \alpha a^3 \quad (18)$$

or

$$a = \frac{d_e}{\sqrt[3]{8\alpha}}. \quad (18a)$$

Note that the centrifugal force is affected significantly by the aspect ratio of the bubble as well as by the bubble size and the bubble rise velocity. The bubble is not stable if F_x is larger than the surface tension force, F_σ, that is,

$$\frac{0.312}{\alpha} \rho_g u_b^2 \left(\frac{d_e}{\sqrt[3]{8\alpha}} \right)^2 \geq 4\sigma \left(\frac{d_e}{\sqrt[3]{8\alpha}} \right) E\left(\sqrt{1-\alpha^2}\right) \quad (19)$$

or

$$u_b^2 d_e \geq \frac{8\alpha^{4/3} E\left(\sqrt{1-\alpha^2}\right)}{0.312} \frac{\sigma}{\rho_g}. \quad (19a)$$

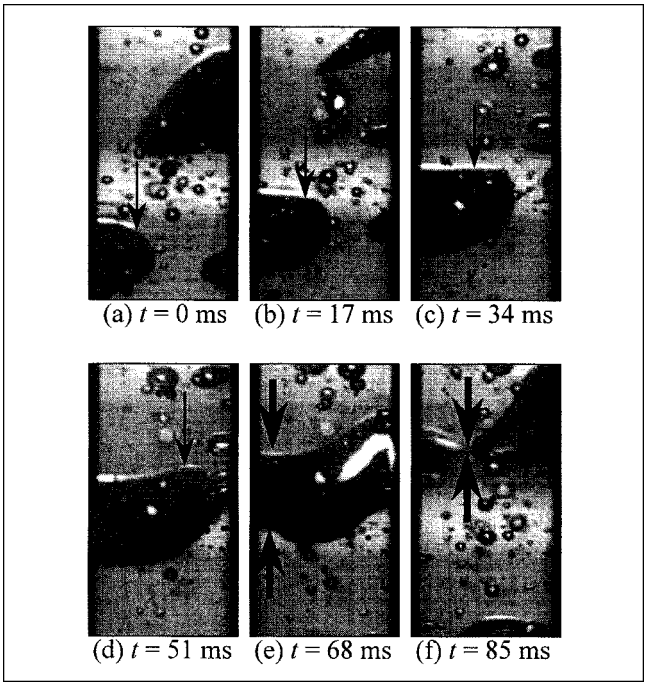

Figure 14. Sequence of bubble images showing the process of bubble breakup (P = 3.5 MPa).

When the centrifugal force is larger than the surface-tension force, the bubble should be stretched in the x-direction. During the stretching, the aspect ratio, α, becomes smaller, while d_e and u_b can be assumed to remain constant. As a result, the centrifugal force increases, the surface-tension force decreases, and the bubble stretching becomes an irreversible process. When the bubble is stretched to an extent where the necking phenomenon occurs, the bubble would split into two smaller bubbles. A sequence of events in the photographs shown in Figure 14 confirm the proposed mechanism of bubble breakup. The bubble images in the figure are obtained at a pressure of 3.5 MPa. It can be seen from the figure that bubble stretching during rising takes place from $t = 0$ to $t = 68$ ms and the necking starts at $t = 68$ ms. At $t = 85$ ms, the bubble splits into two smaller bubbles.

Equation 19a indicates that the breakup of bubbles is dictated by various factors, including bubble size, bubble rise velocity, aspect ratio bubble, gas density, and gas–liquid surface tension. In addition to the direct contribution to the centrifugal force as illustrated by Eqs. 17 and 19, increasing the bubble size also leads to a larger bubble rise velocity and a smaller aspect ratio of the bubble, which both favor bubble breakup. As the pressure increases, the gas density increases and the surface tension decreases; thus, bubbles are less stable.

The bubble rise velocity in high-pressure slurries can be calculated by a correlation developed by Luo et al. (1997b). The simplified form of that correlation for a large bubble is

$$u_b = \sqrt{\frac{2.8\sigma}{\rho_{sl} d_e} + \frac{g d_e}{2} \frac{\rho_{sl} - \rho_g}{\rho_{sl}}}. \quad (20)$$

Equation 20 has a form similar to that of the modified Mendelson equation (Mendelson, 1967) of Maneri (1995), except that the slurry density here is replaced with the liquid density in Maneri's equation. By substituting Eq. 20 into Eq. 19a, d_e can be solved from the resulting equation:

$$d_e \geq \sqrt{\frac{2\sigma}{g}\left[\frac{8\alpha^{4/3}E\left(\sqrt{1-\alpha^2}\right)}{0.312\rho_g}\frac{\rho_{sl}}{\rho_{sl}-\rho_g}-\frac{2.8}{\rho_{sl}-\rho_g}\right]}$$

$$\cong \sqrt{\frac{16\alpha^{4/3}\sigma E\left(\sqrt{1-\alpha^2}\right)}{0.312\, g\,\rho_g}}. \quad (21)$$

Therefore, the maximum stable bubble size is

$$D_{\max} \approx 7.16\alpha^{2/3}E\left(\sqrt{1-\alpha^2}\right)^{1/2}\sqrt{\frac{\alpha}{g\rho_g}}. \quad (22)$$

The aspect ratio of bubble, α, is related to the wake angle, θ_w, by

$$\alpha = \frac{1-\cos\theta_w}{2\sin\theta_w}, \quad (23)$$

and the wake angle for bubbles in liquids depends on the bubble Reynolds number (Clift et al., 1978):

$$\theta_w = 50 + 190\exp\left(-0.62\,Re^{0.4}\right). \quad (24)$$

The wake angle of large bubbles in the liquids can be approximated as 50 deg since the Reynolds number is normally high. The aspect ratio is hence about 0.21 for the large bubbles in liquids, and $E(\sqrt{1-\alpha^2})^{1/2}$ is close to unity. For large bubbles rising in liquid–solids suspensions, the aspect ratio is approximated as 0.3 (Fan and Tsuchiya, 1990) and $E(\sqrt{1-\alpha^2})^{1/2}$ is 1.018. The simplified forms of Eq. 22 are

$$D_{\max} \approx 2.53\sqrt{\frac{\sigma}{g\rho_g}} \qquad (\text{for } \alpha = 0.21) \quad (25a)$$

or

$$D_{\max} \approx 3.27\sqrt{\frac{\sigma}{g\rho_g}} \qquad (\text{for } \alpha = 0.3). \quad (25b)$$

The internal circulation model provides an estimation of the upper limit of the maximum stable bubble size, since the external stresses in the liquid phase are neglected. In actual bubble columns or slurry bubble columns, the observed maximum bubble size should be smaller than the predictions by Eqs. 25a and 25b. Figure 15 shows the comparison between the experimental maximum stable bubble size obtained in the present experimental system and the predictions by different models. The experimental data of maximum stable sizes in Figure 15 are approximated by the maximum bubble sizes

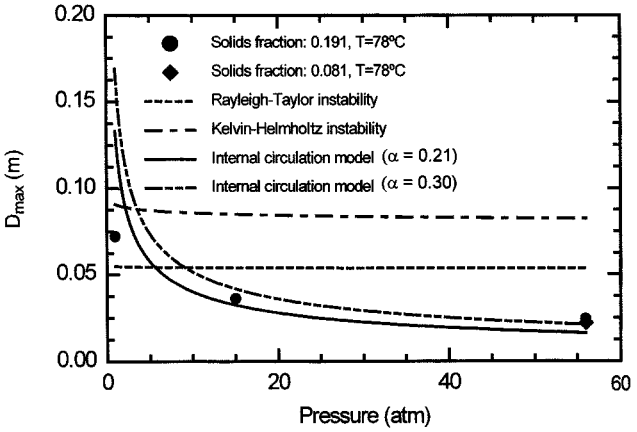

Figure 15. Maximum stable bubble size: experimental data vs. predictions by the internal circulation model.

measured over the entire gas velocity range under the specified pressure, temperature, and solids concentration conditions. The comparison between the predictions and the experimental data indicates that the internal circulation model can reasonably predict the maximum stable bubble size at high pressures in the present experimental system, while the observed effect of pressure on bubble size cannot be explained by the Rayleigh–Taylor instability or the Kelvin–Helmholtz instability. For an air/water system, the prediction by Eq. 25a for the maximum stable bubble size is 5.7 cm at 1.5 MPa, while Wilkinson (1991) observed a maximum bubble size of about 3 cm. However, Eqs. 25a and 25b overpredict the maximum stable size at ambient pressure, as shown in Figure 15. For an air/water system, the predicted maximum stable bubble size is 22 cm and the reported value is 13.2 cm, as discussed earlier. The overprediction by the internal circulation model of this work at ambient pressure suggests that the bubbles are disintegrated by the disturbances in the liquid or slurry through other types of mechanisms, such as, Rayleigh–Taylor instability (Grace et al., 1978) and Kelvin–Helmholtz instability (Kischa and Kocamustafaogullari, 1989), before the bubble size reaches the value predicted by the internal circulation model. It can be seen from Figure 15 that the maximum stable bubble size can be estimated by the internal circulation model at pressures higher than 5 atm; at lower pressures, models based on Rayleigh–Taylor instability (Grace et al., 1978) or Kelvin–Helmholtz instability (Kitscha and Kocamustafaogullari, 1989) should be used. To improve the prediction of the internal circulation model at low pressures, the physical properties of the liquid or the slurry and the external stresses would need to be taken into account.

Based on the internal circulation model, the inertia of the gas and gas–liquid surface tension are the dominant factors dictating the maximum stable bubble size at elevated pressures. The model illustrates an insignificant effect of solids concentration on the maximum bubble size at high pressures since the stresses in the slurry are neglected. At ambient pressure, however, the solids concentration has an indirect effect on the maximum bubble size through the variations of

the shape or the aspect ratio. The maximum stable bubble size would be larger in the slurry than that in the liquid, as exhibited by Eqs. 25a and 25b. Note that the aspect ratio in the slurry (0.3) is larger than that in the liquid (0.21) for a given pressure at high bubble Reynolds numbers.

The importance of the large bubbles to the hydrodynamics in slurry bubble columns can further be manifested through the relationship between the gas holdup correlation, given by Eq. 7, and the rise velocity of the maximum stable bubble, $V_{\max}$, by

$$V_{\max} = \sqrt{\frac{2.8\sigma}{\rho_{sl} D_{\max}} + \frac{gD_{\max}}{2}} \approx 0.71\sqrt{gD_{\max}}. \qquad (26)$$

Substituting Eq. 25a into Eq. 26 yields

$$V_{\max} = 1.1\, g^{1/2} \left(\frac{\sigma}{g\rho_g} \right)^{1/4} \qquad (27a)$$

or

$$V_{\max}^4 = 1.6\, g^2 \frac{\sigma}{g\rho_g} = \frac{1.6\, g\sigma}{\rho_g}. \qquad (27b)$$

Thus, the dimensionless group of $U_g^4 \rho_g / \sigma g$ in Eq. 7 can be rearranged to

$$\frac{U_g^4 \rho_g}{\sigma g} \propto \left(\frac{U_g}{V_{\max}} \right)^4. \qquad (28)$$

Therefore, Eq. 7 can be rearranged to

$$\frac{\epsilon_g}{1-\epsilon_g} \propto \frac{\left(U_g/V_{\max}\right)^{4\alpha} \left(\rho_g/\rho_{sl}\right)^{\beta}}{\cosh\left(Mo_{sl}^{0.054}\right)^{4.1}}. \qquad (29)$$

The gas holdup is thus a function of a set of dimensionless groups, including $U_g/V_{\max}$, Mo_{sl}, and ρ_g/ρ_{sl}. Thus, it is clear that the gas holdup behavior in high-pressure and high-temperature systems can be mimicked using low-pressure and low-temperature systems based on the matching of these dimensionless groups. As the gas holdup is the principal variable that characterizes the hydrodynamic properties of bubble columns or slurry bubble columns, for high-pressure bubble columns and slurry bubble columns operated under the wide range of conditions outlined in Table 3, the hydrodynamic similarity requires these three dimensionless groups to be similar. It is noted that this similarity rule is applicable for columns of diameters greater than 0.1 m and with the column height to diameter ratio larger than 5, under high-pressure batch-liquid operating conditions.

Concluding Remarks

Experiments are conducted to investigate the effect of pressure on the hydrodynamics of a slurry bubble column. The pressure has a significant effect on the gas holdup in the column. The gas holdup increases with pressure and the pressure effect is more pronounced in slurries of higher concentration. The particle concentration also affects the gas holdup, especially at ambient pressure. At elevated pressures, the effect of the solids concentration is relatively small at gas velocities above 25 cm/s. At empirical correlation, which takes into consideration the experimental data obtained from this study and the literature, is developed to account for the gas holdup in both the high-pressure bubble columns and the slurry bubble columns. The correlation covers a wide range of liquid and gas properties, and flow conditions.

To fully understand the effect of pressure on the gas holdup in slurry bubble columns, the bubble flow characteristics during dynamic gas disengagement are analyzed using PIV. The results indicate a dominant effect of large bubbles on bubble rise velocity in slurry bubble columns due to bubble-wake attraction. Without considering bubble-wake attraction, the existing DGD models may severely underestimate the holdup of small bubbles and overestimate the large bubble holdup, and thus lead to errors in estimating the gas-holdup structure and the bubble-size distribution, especially at high gas velocities. The PIV results also indicate that strong bubble–bubble interactions, that is, bubble coalescence and breakup and bubble-wake attraction, exist during the DGD process at ambient and high pressures.

The bubble-size distribution is measured using a fiber-optic probe in the high-pressure slurry bubble column. It is found that bubble size at elevated pressures is significantly smaller than at ambient pressure, under all experimental conditions. The presence of particles in liquids leads to a larger bubble size, especially at ambient pressure. However, the solids concentration does not affect the maximum bubble size at gas velocities above 25 cm/s at 5.6 MPa. An internal circulation model is derived to quantify the observed pressure effect on maximum bubble size. Centrifugal force induced by internal circulation of the gas inside a bubble can disintegrate the bubble at high pressures. As pressure increases, gas inertia increases and surface tension decreases; and therefore the maximum stable bubble size decreases. The model reveals that the gas inertia and gas–liquid surface tension dictate the maximum stable bubble size at high pressures, which explains the relatively small effects of solids concentration on the maximum bubble size and on the gas holdup as observed in this study. A hydrodynamic similarity rule based on the similarity of three dimensionless groups is also proposed for high-pressure operations.

Acknowledgment

Support by National Science Foundation grant CTS-9528380 is greatly acknowledged.

Notation

a = width of ellipse
c = height of ellipse
D_c = column diameter
$d_{b\max}$ = maximum bubble size at a given gas velocity
d_p = particle diameter
g = gravitational acceleration
H = column height
P = pressure
Re = bubble Reynolds number, $\rho_l d_e u_b/\mu_l$
T = temperature

t = time
U_g = superficial gas velocity
U_l = superficial liquid velocity
$\overline{u^2}$ = average value of the squares of velocity differences over a distance of D_{max} across the whole flow field
u_x = x-component of the circulation velocity of gas inside a bubble
z = z-coordinate in a cylindrical coordinate system
α = aspect ratio of bubbles defined in Eq. 18
ϕ = azimuthal angle in spherical coordinates or cylindrical coordinates, or volume fractions of liquid or solids in a slurry
μ = liquid viscosity
θ = polar angle in a spherical coordinate system
σ = gas–liquid surface tension
τ = time period during bubble contact with the probe

Superscript and subscripts

0 = gasfree liquid–solids suspension stage in a dynamic gas disengagement process
d = dynamic pressure
e = volume equivalent

Literature Cited

Akita, K., and F. Yoshida, ''Gas Holdup and Volumetric Mass Transfer Coefficient in Bubble Columns,'' *Ind. Eng. Chem. Process Des. Dev.*, **12**, 76 (1973).

Bach, H. F., and T. Pilhofer, ''Variation of Gas Hold-Up in Bubble Columns with Physical Properties of Liquids and Operating Parameters of Columns,'' *Ger. Chem. Eng.*, **1**, 270 (1978).

Batchelor, G. K., ''The Stability of a Large Gas Bubble Rising through Liquid,'' *J. Fluid Mech.*, **184**, 399 (1987).

Bellman, R., and R. H. Pennington, ''Effect of Surface Tension and Viscosity on Taylor Instability,'' *Q. Appl. Math.*, **51**, 151 (1954).

Chen, R.-C., and L.-S. Fan, ''Particle Image Velocimetry for Characterizing the Flow Structure in Three-Dimensional Gas-Liquid-Solid Fluidized Beds,'' *Chem. Eng. Sci.*, **47**, 3615 (1992).

Chen, Y.-M., and L.-S. Fan, ''On the Criteria of Rayleigh-Taylor Instability at a Curved Interface by a Local Force Balance,'' unpublished results (1988).

Clift, R., J. R. Grace, and M. E. Weber, *Bubbles, Drops, and Particles*, Academic Press, New York (1978).

Daly, J. G., S. A. Patel, and D. B. Bukur, ''Measurement of Gas Holdups and Sauter Mean Bubble Diameters in Bubble Column Reactors by Dynamic Gas Disengagement Method,'' *Chem. Eng. Sci.*, **47**, 3647 (1992).

de Lasa, H., S. L. P. Lee, and M. A. Bergougnou, ''Bubble Measurement in Three-Phase Fluidized Beds Using a U-Shaped Optical Fiber,'' *Can. J. Chem. Eng.*, **62**, 1029 (1982).

de Swart, J. W. A., R. F. van Vliet, and R. Krishna, ''Size, Structure, and Dynamics of 'Large' Bubbles in a Two-Dimensional Slurry Bubble Column,'' *Chem. Eng. Sci.*, **51**, 4619 (1996).

Deckwer, W.-D., Y. Louisi, A. Zaidi, and M. Ralek, ''Hydrodynamic Properties of the Fischer-Tropsch Slurry Process,'' *Ind. Eng. Chem. Process Des. Dev.*, **19**, 699 (1980).

Deckwer, W.-D., *Bubble Column Reactors*, Wiley, Chichester, England (1992).

Deckwer, W.-D., and A. Schumpe, ''Improved Tools for Bubble Column Reactor Design and Scale-up,'' *Chem. Eng. Sci.*, **48**, 889 (1993).

Desphande, N. S., M. Dinkar, and J. B. Joshi, ''Disengagement of the Gas Phase in Bubble Columns,'' *Int. J. Multiphase Flow*, **21**, 1191 (1995).

Fan, L.-S., *Gas-Liquid-Solid Fluidization Engineering*, Butterworths, Stoneham, MA (1989).

Fan, L.-S., and K. Tsuchiya, *Bubble Wake Dynamics in Liquids and Liquid-Solid Suspensions*, Butterworth-Heinemann, Stoneham, MA (1990).

Fox, J. M., ''Fischer-Tropsch Reactor Selection,'' *Catal. Lett.*, **7**, 281 (1990).

Fu, W., Y. Chisti, and M. Moo-Young, ''A New Method for the Measurement of Solids Holdup in Gas-Liquid-Solid Three Phase Systems,'' *Ind. Eng. Chem. Res.*, **34**, 928 (1995).

Grace, J. R., T. Wairegi, and J. Brophy, ''Break-Up of Drops and Bubbles in Stagnant Media,'' *Can. J. Chem. Eng.*, **56**, 3 (1978).

Hill, M. J. M., ''On a Spherical Vortex,'' *Philos. Trans. Roy. Soc. London*, **185**, 213 (1894).

Hinze, J. O., ''Fundamentals of the Hydrodynamic Mechanism of Splitting in Dispersion Processes,'' *AIChE J.*, **1**, 289 (1955).

Idogawa, K., K. Ikeda, T. Fukuda, and S. Morooka, ''Behavior of Bubbles of the Air-Water System in a Column under High Pressure,'' *Int. Chem. Eng.*, **26**, 468 (1986).

Inga, J. R., ''Scaleup and Scaledown of Slurry Reactors: A New Methodology,'' PhD Thesis, Univ. of Pittsburgh, Pittsburgh, PA (1997).

Jiang, P., T.-J. Lin, X. Luo, and L.-S. Fan, ''Flow Visualization of High Pressure (21 MPa) Bubble Column: Bubble Characteristics,'' *Trans. Inst. Chem. Eng.*, **73** (Part A), 269 (1995).

Kastaneck, F., J. Zahradnik, J. Kratochvil, and J. Cermak, ''Modelling of Large-Scale Bubble Column Reactors for Non-Ideal Gas-Liquid Systems,'' *Frontiers in Chemical Reaction Engineering*, L. K. Doraiswamy, and R. A. Mashelkar, eds., Vol. 1, Whiley, Bombay, India, p. 330 (1984).

Kitscha, J., and G. Kocamustafaogullari, ''Breakup Criteria for Fluid Particles,'' *Int. J. Multiphase Flow*, **15**, 573 (1989).

Koide, K., A. Takazawa, and M. Komura, ''Gas Holdup and Volumetric Liquid-Phase Mass Transfer Coefficient in Solid-Suspended Bubble Columns,'' *J. Chem. Eng. Jpn.*, **17**, 459 (1984).

Kojima, H., B. Okumura, and A. Nakamura, ''Effect of Pressure on Gas Holdup in a Bubble Column and a Slurry Bubble Column,'' *J. Chem. Eng. Jpn.*, **24**, 115 (1991).

Krishna, R., P. M. Wilkinson, and L. L. van Dierendonck, ''A Model for Gas Holdup in Bubble Columns Incorporating the Influence of Gas Density on Flow Regime Transitions,'' *Chem. Eng. Sci.*, **46**, 2491 (1991).

Krishna, R., J. W. A. de Swart, J. Ellenberger, G. B. Martina, and C. Maretto, ''Gas Holdup in Slurry Bubble Columns: Effect of Column Diameter and Slurry Concentrations,'' *AIChE J.*, **43**, 311 (1997).

Lee, D. J., X. Luo, and L.-S. Fan, ''Gas Disengagement Technique in a Slurry Bubble Column Operated in the Coalesced Bubble Regime,'' Int. Symp. of Chemical Reaction Engineering, Newport Beach, CA (1998).

Levich, V. G., *Physiochemical Hydrodynamics*, Prentice-Hall, Englewood Cliffs, NJ (1962).

Li, H., and A. Prakash, ''Heat Transfer and Hydrodynamics in a Three-Phase Slurry Bubble Column,'' *Ind. Eng. Chem. Res.*, **36**, 4688 (1997).

Lin, T.-J., K. Tsuchiya, and L.-S. Fan, ''Bubble Flow Characteristics in Bubble Columns at Elevated Pressure and Temperature,'' *AIChE J.*, **44**, 545 (1998).

Liu, W., N. N. Clark, and A. I. Karamavruc, ''General Method for the Transformation of Chord-Length Data to a Local Bubble-Size Distribution,'' *AIChE J.*, **42**, 2713 (1996).

Luo, X., P. Jiang, and L.-S. Fan, ''High Pressure Three-Phase Fluidization: Hydrodynamics and Heat Transfer,'' *AIChE J.*, **43**, 2432 (1997a).

Luo, X., J. Zhang, K. Tsuchiya, and L.-S. Fan, ''On the Rise Velocity of Bubbles in Liquid-Solid Suspensions at Elevated Pressure and Temperature,'' *Chem. Eng. Sci.*, **52**, 3693 (1997b).

Maneri, C. C., ''New Look at Wave Analogy for Prediction of Bubble Terminal Velocities,'' *AIChE J.*, **41**, 481 (1995).

Mendelson, H. D., ''The Prediction of Bubble Terminal Velocities from Wave Theory,'' *AIChE J.*, **13**, 250 (1967).

O'Dowd, W., D. N. Smith, J. A. Ruether, and S. C. Saxena, ''Gas and Solids Behavior in a Baffled and Unbaffled Slurry Bubble Column,'' *AIChE J.*, **33**, 1959 (1987).

Oyevaar, M., ''Gas-Liquid Contacting at Elevated Pressures,'' PhD Thesis, Twente Univ., Twente, The Netherlands (1989).

Patel, S. A., J. Daly, and D. Bukur, ''Holdup and Interfacial Area Measurements using Dynamic Gas Disengagement,'' *AIChE J.*, **35**, 931 (1989).

Petukhov, V. I., and V. A. Kolokol'tsev, ''Effect of Liquid Viscosity on Droplet Entrainment and Volumetric Air Content,'' *Therm. Eng.*, **12**, 41 (1965).

Reilly, I. G., D. S. Scott, T. J. W. de Bruijn, and D. MacIntrye, ''The Role of Gas Phase Momentum in Determining Gas Holdup and

Hydrodynamic Flow Regimes in Bubble Column Operations,'' *Can. J. Chem. Eng*., **72**, 3 (1994).
Saxena, S. C., R. Vadivel, and A. C. Saxena, ''Gas Holdup and Heat Transfer from Immersed Surfaces in Two- and Three-Phase Systems in Bubble Columns,'' *Chem. Eng. Commun.*, **85**, 63 (1989).
Saxena, S. C., and Z. D. Chen, ''Hydrodynamics and Heat Transfer of Baffled and Unbaffled Slurry Bubble Columns,'' *Rev. Chem. Eng*., **10**, 193 (1994).
Saxena, S. C., ''Bubble Column Reactors and Fischer-Tropsch Synthesis,'' *Catal. Rev.-Sci. Eng*., **37**, 227 (1995).
Schumpe, A., and G. Grund, ''The Gas Disengagement Technique for Studying Gas Holdup Structure in Bubble Columns,'' *Can. J. Chem. Eng*., **64**, 891 (1986).
Shah, Y. T., B. G. Kelkar, S. P. Godbole, and W.-D. Deckwer, ''Design Parameters Estimations for Bubble Column Reactors,'' *AIChE J*., **28**, 353 (1982).
Shollenberger, K. A., and T. J. O'Hern, ''Characterization of Slurry-Phase Flow in the LaPorte Alternative Fuels Development Unit (AFDU) Using Differential Pressure Measurements,'' U.S. DOE Rep., Washington, DC (1997).
Sriram, K., and R. Mann, ''Dynamic Gas Disengagement: A New Technique for Assessing the Behaviour of Bubble Columns,'' *Chem. Eng. Sci*., **32**, 571 (1977).
Tarmy, B., M. Chang, C. Coulaloglou, and P. Ponzi, ''Hydrodynamic Characteristics of Three Phase Reactors,'' *Chem. Eng*., 18 (1984).
Vermeer, D. J., and R. Krishna, ''Hydrodynamics and Mass Transfer in Bubble Columns Operating in the Churn-Turbulent Regime,'' *Ind. Eng. Chem. Process Des. Dev*., **20**, 475 (1981).
Walter, J. F., and H. W. Blanch, ''Bubble Break-Up in Gas-Liquid Bioreactors: Break-Up in Turbulent Flows,'' *Chem. Eng. J*., **32**, B7 (1986).
Wilkinson, P., and L. L. van Dierendonck, ''Pressure and Gas Density Effects on Bubble Break-Up and Gas Holdup in Bubble Columns,'' *Chem. Eng. Sci*., **8**, 2309 (1990).
Wilkinson, P. M., ''Physical Aspects and Scale-Up of High Pressure Bubble Columns,'' PhD Thesis, Univ. of Groningen, Groningen, The Netherlands (1991).
Wilkinson, P., A. P. Spek, and L. L. van Dierendonck, ''Design Parameters Estimation for Scale-Up of High Pressure Bubble Columns,'' *AIChE J*., **38**, 544 (1992).

Manuscript received Oct. 27, 1998, and revision received Jan. 4, 1999.